Accepted Manuscript

High-Q microwave dielectric properties in the $Na_{0.5}Sm_{0.5}TiO_3$ + Cr_2O_3 ceramics by one synthetic process

Zi-xuan Fang, Bin Tang, Enzhu Li, Shu-ren Zhang

PII: S0925-8388(17)30234-7

DOI: 10.1016/j.jallcom.2017.01.200

Reference: JALCOM 40567

To appear in: *Journal of Alloys and Compounds*

Received Date: 3 October 2016

Revised Date: 16 January 2017

Accepted Date: 19 January 2017

Please cite this article as: Z.-x. Fang, B. Tang, E. Li, S.-r. Zhang, High-Q microwave dielectric properties in the $Na_{0.5}Sm_{0.5}TiO_3$ + Cr_2O_3 ceramics by one synthetic process, *Journal of Alloys and Compounds* (2017), doi: 10.1016/j.jallcom.2017.01.200.

Graphical Abstract

The experimental XPS results showed that Cr^{3+} substitution restrained the formation of Ti^{3+} ions in the $Na_{0.5}Sm_{0.5}TiO_3$ + Cr_2O_3 ceramics by one synthetic process

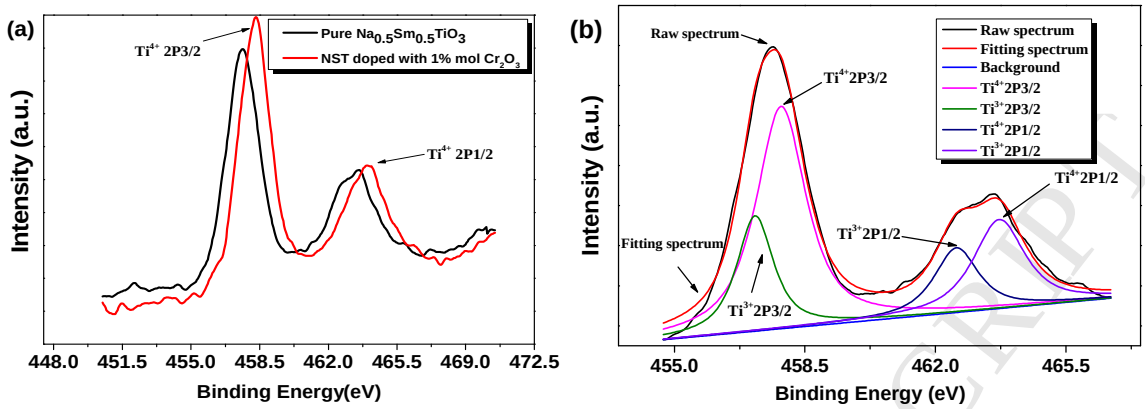

Fig. 6. (a) The experimental spectrum of Ti 2p for pure $Na_{0.5}Sm_{0.5}TiO_3$ and NST ceramics doped with 1% mol Cr_2O_3, and (b) the experimental and deconvoluted Ti 2p XPS spectrum for pure $Na_{0.5}Sm_{0.5}TiO_3$ ceramics sintered at 1450°C for 2 h.

High-Q Microwave Dielectric Properties in the $Na_{0.5}Sm_{0.5}TiO_3$ + Cr_2O_3 Ceramics by One Synthetic Process

Zi-xuan Fang [1,2] Bin Tang [1,2]* Enzhu Li[1,2] Shu-ren Zhang[1,2]

1. National Engineering Center of Electromagnetic Radiation Control Materials, University of Electronic Science and Technology of China, Jianshe Road, Chengdu 610054, P.R. China
2. State Key Laboratory of Electronic Thin Films and Integrated Devices, University of Electronic Science and Technology of China, Jianshe Road, Chengdu 610054, P.R. China

*Corresponding author: tangbin@uestc.edu.cn

Abstract:

The $Na_{0.5}Sm_{0.5}TiO_3$ + x mol Cr_2O_3 ceramics (x = 0, 0.25%, 0.5%, 0.75%, 1%, 1.25% and 1.5%) were conventionally prepared using solid-state reaction method by one synthesizing process. All specimens were identified as a structure of orthorhombic perovskite with Pnma space group. Both of XRD patterns and refinement results showed that the Cr^{3+} had incorporated into the lattice at Ti sites, leading to the expansion of cell volume. The densification can be improved by adding a proper amount of Cr_2O_3 (0.25%$\leqslant x\leqslant$1%). The permittivity (ε_r) slightly increased with $x\leqslant$0.25%, later decreased with further addition of Cr_2O_3, which showed a similar varying trend to dielectric polarizabilities. The temperature coefficient of the resonant frequency (τ_f) was reduced from 199.3 ppm/°C to 160.8 ppm/°C due to an increase of B-site bond valence. The experimental XPS results confirmed that there was a significant increase of quality factor ($Q\times f$) from 8993 GHz at x = 0 to 11854 GHz at x = 1% due to the restraint of Ti^{4+} reduction to Ti^{3+}. When added with 1% mol Cr_2O_3, the $Na_{1/2}Sm_{1/2}TiO_3$ ceramic sintered at 1450°C for 2h exhibited high microwave dielectric properties of ε_r=96, $Q\times f$=11854 GHz and τ_f=171.2 ppm/°C.

Keywords: Dielectric loss; Dielectrics; perovskite; XPS

1. Introduction

With the advent of 5G technology in wireless communication, the demand for microwave dielectric ceramics with high performance has increased dramatically because of their paramount roles in microwave applications, such as satellites and any hand-held terminals. Recent decades, researchers have made great strides in finding plenty of microwave ceramic systems with a high dielectric constant (ε_r), high quality factor ($Q\times f$) and adjustable temperature coefficient of the resonant frequency (τ_f), such as Li_2O-BO-TiO_2 (B=Zn^{2+}, Mg^{2+}), A($B'_{1/3}B''_{2/3}$)O_3 (A=Ba, Ca, B′=Zn^{2+}, Mg^{2+}, Co^{2+} and Ni^{2+}, B″=Ta, Nb) ceramics, and BaO-Ln_2O_3-TiO_2 (Ln=rare earth) [1-4]. Although these ceramics have excellent microwave performance, their dielectric permittivities mainly varied

in the range of 10 to 80 which are not competent to meet the further demand of miniaturization.

As a member of the series of $Na_{0.5}Ln_{0.5}TiO_3$ (Ln=La, Nd and Sm) microwave ceramics, the $Na_{0.5}Sm_{0.5}TiO_3$ (NST) ceramic system presents a high dielectric permittivity (ε_r=100.5), high quality factor ($Q\times f$=8993GHz) [5-7]. Because of the high permittivity, the orthorhombic perovskite structured $Na_{0.5}Sm_{0.5}TiO_3$ ceramics are considered as promising candidates in miniaturizing microwave dielectric devices [6]. In many reports of Ti based ceramic systems [8-11] , however, it is common to find the serious deterioration in microwave dielectric loss owing to the reduction of Ti^{4+} to Ti^{3+} in high sintering temperature. As known to us, the reduction of Ti^{4+} to Ti^{3+} is detrimental for $Na_{0.5}Sm_{0.5}TiO_3$ to be used as resonator materials. And the efforts to restrain the reduction of Ti^{4+} have been an active field recently. The dielectric loss will be greatly decreased by doping with a range of divalent and trivalent acceptor cations with ionic radii between 0.5 Å and 0.95Å, such as Zn^{2+}, Mg^{2+}, Mn^{2+}, Cu^{2+}, Co^{2+}, Mn^{3+}, Cr^{3+}, Al^{3+} and B^{3+}. For example, Pullar et al [9]. revealed that the “dark hole” can be cured by adding these cations into TiO_2 ceramics, and a dramatic improvement of ε_r and $Q\times f$ could be obtained. Huang et al. [8] reported that a significant increase of quality factor was achieved by adding Mn^{2+}, Cu^{2+} and Co^{2+} into $Ba_{4.2}Nd_{9.2}Ti_{18}O_{54}$ ceramics. Fang et al. [11] claimed that a proper amount of Al^{3+} substitution for Ti^{4+} was beneficial to improve the quality factors due to the restraint of Ti^{4+} reduction; it influenced the variation of ε_r and τ_f through changing its B-site bond valence in Ca-Li-Nd-Ti system. It was meaningful for Guo et al. [10] to find that the substitution of Cr^{3+} for Ti^{4+} restrained the reduction of Ti^{4+} to Ti^{3+} in $Ba_{6-3x}Nd_{8+2x}Ti_{18}O_{54}$ ceramics while maintaining its high permittivities. To date, a small amount of studies for $Na_{0.5}Sm_{0.5}TiO_3$ system have been confined to improve its basic synthesizing process and tune its τ_f. But no attentions have been paid to combat the reduction of Ti^{4+} to Ti^{3+} in NST ceramics.

In this study, the $Na_{0.5}Sm_{0.5}TiO_3$ + x mol Cr_2O_3 ceramics (x = 0, 0.25%, 0.5%, 0.75%, 1%, 1.25% and 1.5%) were synthesized by one synthetic process in order to improve quality factor and maintain high permittivity. Meanwhile, the effects of Cr^{3+} ions on the crystal structures, microstructures and microwave dielectric characteristics of $Na_{0.5}Sm_{0.5}TiO_3$ were investigated systematically by using XRD, SEM and XPS technology.

2. Experimental procedures

Specimens of $Na_{1/2}Sm_{1/2}TiO_3$ + *x* mol Cr_2O_3 ceramics (*x* = 0, 0.25%, 0.5%, 0.75%, 1%, 1.25% and 1.5%) were prepared by one synthetic process using the conventional solid-state ceramic route. The raw materials were Na_2CO_3 (ChengDu Kelong Chemical Co., Ltd, Chengdu, China), Sm_2O_3 (Gansu Rare-earth New Materials Co., Ltd, Baiyin, China), Cr_2O_3 (ChengDu Kelong Chemical Co., Ltd, Chengdu, China) and TiO_2 (Xiantao ZhongXing Electric Co., Ltd, Xiantao, China) with at least 99.9 % purity. The starting oxide materials were weighted according to the stoichiometry proportions with addition of 6 wt % Na_2CO_3 powder because of the serious evaporation of sodium in high temperature. The mixture of starting materials was ball-milled in alcohol medium for 5 h in nylon jar using zirconia balls. The mixed slurry was dried, passed through a100-mesh sieve, later, calcined in air at 1150 °C for 3 h. The fine powder was mixed with a 6 wt. % of a 10% solution of polyvinyl alcohol (PVA) as a binder. The obtained powder was axially pressed into cylindrical disks with thickness of 7.5 mm and 15 mm in a diameter under a pressure of 20 MPa. These samples were first heated at 600 °C for 3 h to burn out the organic binder, later, these pellets were sintered at 1450 °C for 2 h in air.

After sintering, the apparent densities of the samples were measured using the Archimedes method. The powder phase composition were examined by X-ray diffraction (XRD) using CuKα radiation (Philips x'pert Pro MPD, Netherlands) and the refined lattice parameters of samples were collected by analyzing XRD data using the Maud software. The chemical compositions of $Na_{0.5}Sm_{0.5}TiO_3$ + *x* mol Cr_2O_3 ceramic powder (*x*=0, 0.75% and 1.5%) were measured by the x-ray fluorescence. The reliability of the refined results was evaluated by the pattern R factors (*Rw* (weight profile), *Rwnb* (an value similar to that reported for single-crystal refinements), *Rb* (the Bragg-intensity R value) and *Rexp* (the quality of the data)). The visualization of crystal structure of NST ceramics was obtained by VESTA software [12]. Scanning electron microscopy (SEM) (FEI Inspect F, United Kingdom) was employed to study the thermally etched surface morphology of the specimens. The valence of Ti ion was identified by X-ray photoelectron spectroscopy (XPS) (Thermo scientific ESCALAB 250Xi). The dielectric characteristics at microwave frequencies were measured by the Hakki–Coleman dielectric resonator method in the TE011 mode using a network analyzer (Agilent Technologies E5071C, USA) and a temperature chamber (DELTA 9023, Delta Design, USA). The temperature coefficients of resonant frequency were calculated by equation:

$\tau_f = (f_{t_2} - f_{t_1})/(f_{t_1} \times (t_2 - t_1))$ (1), where f_{t_1} and f_{t_2} were the resonant frequencies at the measuring temperature t_1 (25 °C) and t_2 (85 °C), respectively.

3. Results and discussions

Fig. 1(a) illustrates XRD patterns of powder $Na_{1/2}Sm_{1/2}TiO_3$ + *x* mol Cr_2O_3 ceramics (*x*=0 to 1.5%) sintered at 1450°C for 2 h in air. For all compositions, the main peaks of samples were confirmed as a structure of orthorhombic perovskite, and no peaks for secondary phase can be detected, which implied that Cr^{3+} ions had incorporated into the crystal lattices and formed solid solutions. Weak superlattice reflections, as previously reported in literature [13, 14], were also observed for all compositions in this investigation. These weak peaks were indexed as (1, 1/2, 0), (1,1,1/2), (3/2, 1/2, 1/2), (2, 1/2, 0), (3/2, 3/2, 1/2), (2, 1, 1/2) and (2, 1, 3/2), which were in even-even-odd and odd-odd-odd manners [13, 15]. Furthermore, Glazer's investigation [16, 17] revealed that these doubled index superlattice reflections also existed in $CaTiO_3$ with tiltings of oxygen octahedra, which was suggested as a space group *Pnma*. On a close examination, the characteristic peaks slightly shifted to lower angles of 2θ, which indicated that an increase of cell volume happened. Therefore, the Rietveld refinement method were carried out on the basis of the X-ray diffraction data of all sintered samples.

The experimental and calculated X-ray diffraction patterns of Cr added specimens are given in Fig. 2 with (a) *x*= 0 and (b) *x*= 1%. Both of them were confirmed as a structure of orthorhombic perovskite with *Pnma* space group, and the doubled-index superlattice reflections were fitted very well. The detailed lattice parameters and *R* values of all samples are presented in Table 1. As seen from Table. 1, the cell volumes steadily increased as the Cr^{3+} increased because the small Ti^{4+} ion (0.605 Å) was substituted by a relatively larger Cr^{3+} ion (0.615 Å). To further comprehend the crystal structure, perovskite structure of pure NST ceramics can be visually displayed on illustrations drawn by utilizing the refined structural parameters. Figure 3 depicts the schematic representation of (a) $Na_{0.5}Sm_{0.5}TiO_3$ with perovskite structure and (b) the c-axis was chosen as the long axis. As shown in Fig. 3, the A site was occupied by Na, Sm and vacancies, and TiO6 octahedron occupied layers between the A site ones, which formed periodic structures [18, 19]. And the superstructure reflections originated from the A-site ordering (periodic structure). According the Inaguma et al [15] and Sun et al's [13] researches, the weak peaks ((3/2, 1/2, 1/2) and

(3/2, 3/2, 1/2)) can be detected in the $La_{1/2}Na_{1/2}TiO_3$. And when La was replaced by Pr, Nd, Sm and other small rare earths, other five weak peaks were detected, which can be indexed as (1, 1/2, 0), (1, 1, 1/2), (2, 1/2, 0), (2, 1, 1/2) and (2, 1, 2/3). These double index of the above reflections ((1, 1/2, 0), (1,1,1/2), (3/2, 1/2, 1/2), (2, 1/2, 0), (3/2, 3/2, 1/2), (2, 1, 1/2) and (2, 1, 3/2)) was in an even-even-odd and odd-odd-odd manner. The substitution of Cr for Na/Sm in the NST ceramics was not able to meet the requirement for formation of a solid solution as the difference in ionic radius between Na/Sm (1.33 Å) and Cr^{3+} (0.615 Å) was much larger than 15% [20]. Therefore, it was impossible for Cr^{3+} to substitute for Na/Sm ions at A-sites. As discussed above, the results showed that Cr^{3+} had incorporated into the lattice at B-sites and formed a solid solution. We also carried out the measures of the x-ray fluorescence (XRF) of $Na_{0.5}Sm_{0.5}TiO_3$ + *x* mol Cr_2O_3 ceramic powder. Table 2 lists the representative chemical compositions of $Na_{0.5}Sm_{0.5}TiO_3$ + *x* mol Cr_2O_3 ceramic powder (*x*=0, 0.75% and 1.5%) sintered at 1450 ^oC for 2 h. After converting the weight ration to mole ration, as we can see, the Na/Sm/Ti atomic ratios of samples were determined by XRF analysis to be about 1: 1: 2. And the concentration of Cr steadily increased.

Figure 4 shows SEM photographs of $Na_{0.5}Sm_{0.5}TiO_3$ + *x* mol Cr_2O_3 ceramics sintered at 1450 °C for 2 h with (a) *x* = 0 to (g) *x* = 1.5%. There were two big changes of the microstructure when the Cr_2O_3 were added. One change was that a certain amount of pores shown in Fig. 4(a) could be effectively eliminated by adding Cr_2O_3 and the compact microstructure with crystal grains in dense contact could be obtained with *x*=0.25% to 1%. But pores were observed again in Fig. 4(f)~(g), as superfluous Cr ($x \geq 1.25\%$) were added. Another one was that the increase of Cr_2O_3 were beneficial to promote the grain growth, and when $x \leqslant 1\%$, the microstructure gradually became uniform. Apparently, a high densification was achieved and the homogeneous microstructure was observed at *x* = 1%.

Figure 5 shows the (a) relative density, (b) dielectric constant (c) temperature coefficient of resonant frequency and (d) quality factor of $Na_{0.5}Sm_{0.5}TiO_3$ + *x* mol Cr_2O_3 ceramics (*x*=0 to 1.5%) sintered at 1450^{o}C for 2 h. The theoretical density and relative density are presented in Table 2. As shown Fig. 5 (a) and Table 3, when $x \leqslant 1\%$, there was a steady increase of relative density of samples which was primarily resulted from the elimination of pores pined at the boundary of matrix grains. However, when *x* exceeded 1%, relative density decreased and it was mainly caused by the appearance of pores and increase of cell volume, as shown in Fig. 4 (f)~(g) and Table 3. As

clearly listed in Table 3, all samples presented high relative densities which were higher than 94%. The presence of some small pores in one of the samples in Fig. 4 did not necessarily make the density poor. This may be attributable to a slightly different sintering schedule followed, such as a little longer soaking or faster heating [11]. Occasional porosity at the grain boundaries did not make the density extremely poor for x=0, 1.25% and 1.5%. With 0.25%$\leqslant$ $x\leqslant$1%, a proper amount of Cr_2O_3 could improve the densification of NST ceramics to some extent.

For ε_r shown in Fig. 5 (b), it slightly increased with $x\leqslant$0.25%, later decreased with further addition of Cr_2O_3. In general, the dielectric constant is closely related to the relative density, pores, ionic polarizabilities. As the relative density of all Cr-added samples was larger than 94%, the ε_r of dielectrics was mainly dependent on dielectric polarizabilities [21, 22]. The dielectric polarizabilities was calculated by Clausius–Mosotti equation as formulated in eqn (2) with measured dielectric constant at microwave frequencies [1]. The dielectric polarizabilities are listed in Table 3 as well as molar volumes and dielectric constant. $\alpha_D = \frac{V_m(\varepsilon_r-1)}{b(\varepsilon_r-2)}$ (2), where V_m, ε_r and b indicated the molar volume of samples, dielectric constant and constant value ($4\pi/3$). As shown in Table 3, the dielectric constant presented a similar trend to dielectric polarizabilities.

Figure 5 (c) presents the τ_f and B-site bond valence (V_B) as a function of Cr_2O_3. As is known, the τ_f of the ABO_3 type perovskite is widely considered to be influenced by secondary phase and tiliting of oxygen octahedra [23]. Because of the single phase of all Cr added NST ceramics, the tiliting of oxygen octahedra played key role to affect the τ_f. And the oxygen octahedra was closely related to the B-site bond valence $\left(V_{Ti,Cr-O}\right)$. The B-site bond valence (V_B) is based on the equation: $V_i = \sum_{i=1}^{n=6} v_{ij}$ (3), and $v_{ij} = \exp\left(\frac{R_{ij}-d_{ij}}{b'}\right)$ (4), where R_{ij} is the bond valence parameter, d_{ij} is the length of a bond between atom i and j, and b' is commonly taken to be a universal constant equal to 0.37 Å. The τ_f and V_B are also displayed in Table 4. Obviously, the τ_f was reduced from 199.3 ppm/°C to 160.8 ppm/°C due to an increase of B-site bond valence.

As shown in Fig. 5 (d), there was a significant increase of $Q\times f$ from 8993 GHz at x = 0 to 11854 GHz at x = 1% but a big drop to 9241GHz at x = 1.5% was observed. The changing tendency of $Q\times f$ was in accordance with the trend between density and Cr_2O_3 because both of the density and $Q\times f$ values were much influenced by the same reasons such as densification and pores [24]. Moreover, the pure NST ceramics had very low $Q\times f$ value because the Ti^{4+} attracted unwanted electrons and

transformed into Ti^{3+} in such high temperature, $O_o \rightarrow V_{\ddot{O}} + 2e' + \frac{1}{2}O_2$ (5), $e' + Ti^{4+} \rightarrow Ti^{3+}$ (6). But the introduction of Cr^{3+} would effectively restrain Ti^{4+} reduction, contributing to improvement of $Q\times f$, $Cr^{3+} + Ti^{3+} \rightarrow Cr^{2+} + Ti^{4+}$ (7). Figure 6 shows (a) the experimental XPS spectrum of Ti 2p for pure $Na_{1/2}Sm_{1/2}TiO_3$ ceramics and $Na_{1/2}Sm_{1/2}TiO_3$ + 1% mol Cr_2O_3 ceramics, and (b) the experimental and deconvoluted Ti 2p XPS spectrum for pure $Na_{1/2}Sm_{1/2}TiO_3$ ceramics sintered at 1450°C for 2 h. The Ti $2p_{3/2}$ and Ti $2p_{1/2}$ spin-orbital splitting photoelectrons of Cr added NST ceramics were located at binding energies of around 458 and 464 eV, respectively, indicating that Ti existed as Ti^{4+} [25, 26]. When no Cr_2O_3 were added, moving towards lower binding energies was observed, and shoulder regions were revealed at approximately 456 eV and 464 eV. These shoulder peaks could be ascribed to Ti^{3+} $2p_{3/2}$ and Ti^{3+} $2p_{1/2}$, implying the presence of Ti^{3+} in the pure NST samples. As shown in Fig. 6(b), the fitting and deconvoluted Ti 2p XPS spectrum strongly demonstrated that the Ti^{4+} and Ti^{3+} co-existed in pure NST ceramics. Therefore, the significant improvement of $Q\times f$ was mainly due to the restraint of Ti^{4+} reduction to Ti^{3+} as the Cr_2O_3 were added.

In summary, the microwave dielectric properties of NST + Cr_2O_3 ceramics were strongly determined by the Cr_2O_3. The τ_f sharply decreased from 199.3 ppm/°C to 160.8 ppm/°C owing to the increase of B-site bond valence. The ε_r initially increased, and then decreased, which showed a similar tendency to dielectric polarizabilities. The $Q\times f$ could be significantly improved to 11854 GHz at x = 1% mainly because of the restraint of Ti^{4+} reduction. Hence, when sintered at 1450°C for 2h, the $Na_{1/2}Sm_{1/2}TiO_3$ ceramic with 1% mol Cr_2O_3 exhibited the microwave dielectric properties of ε_r=96, $Q\times f$=11854 GHz and τ_f=171.2 ppm/°C.

4. Conclusions

The $Na_{0.5}Sm_{0.5}TiO_3$ + x mol Cr_2O_3 ceramics were conventionally synthesized by one synthetic process. Meanwhile, the effects of Cr^{3+} ions on the microstructures and microwave dielectric characteristics of $Na_{0.5}Sm_{0.5}TiO_3$ were investigated systematically. All specimens were identified as a structure of orthorhombic perovskite with $Pnma$ space group. Both of XRD patterns and its refinement results showed that the Cr^{3+} had incorporated into the lattice at Ti sites, leading to the expansion of cell volume. The microstructure and densification can be improved by adding a proper amount of Cr_2O_3 dopants (0.25%$\leqslant x\leqslant$1%). The ε_r slightly increased with $x\leqslant$0.25%, but later

decreased with further addition of Cr_2O_3, which showed a similar varying trend to dielectric polarizabilities. The τ_f was significantly reduced from 199.3 ppm/°C to 160.8 ppm/°C due to an increase of B-site bond valence. It was remarkable that there was a significant increase of $Q \times f$ from 8, 993 GHz at x = 0 to 11854 GHz at x = 1%, which was mainly attributable to the restraint of Ti^{4+} reduction to Ti^{3+}. When added with 1% mol Cr_2O_3 dopants, the $Na_{1/2}Sm_{1/2}TiO_3$ ceramic sintered at 1450°C for 2h exhibited the microwave dielectric properties of ε_r=96, $Q \times f$=11854 GHz and τ_f =171.2 ppm/°C.

Acknowledgement

This work was supported by the Open Foundation of National Engineering Research Center of Electromagnetic Radiation Control Materials (ZYGX2016K003-5)

References

[1] Y. Zhao, P. Zhang, J Alloys Compd. 658 (2016) 744-748.

[2] H. Wu, E.S. Kim, RSC Adv. 6 (2016) 47443-47453.

[3] E. Kenichi, B. Yoko, T. Hisakazu, S. Kenichi, N. Shoichi, Jpn J Appl Phys. 32 (1993) 4319.

[4] H. Ohsato, J Eur Ceram Soc. 21 (2001) 2703-2711.

[5] M.T. Sebastian, Dielectric materials for wireless communication. 2010: Elsevier.

[6] Z.-x. Fang, B. Tang, F. Si, S.-r. Zhang, J Mater Sci: Mater Electron. (2015) 1-7.

[7] H. Takahashi, Y. Baba, K. Ezaki, Y. Okamoto, K. Shibata, K. Kuroki, S. Nakano, Jpn J Appl Phys. 30 (1991) 2339.

[8] B. Huang, Z. Yan, X. Lu, L. Wang, Z. Fu, Q. Zhang, Ceram. Int. 42 (2016) 10758-10763.

[9] R.C. Pullar, S.J. Penn, X. Wang, I.M. Reaney, N.M. Alford, J Eur Ceram Soc. 29 (2009) 419-424.

[10] X. Guo, B. Tang, J. Liu, H. Chen, S. Zhang, J Alloys Compd. 646 (2015) 512-516.

[11] Z. Fang, B. Tang, F. Si, S. Zhang, J Alloys Compd. 693 (2017) 843-852.

[12] K. Momma, F. Izumi, J Appl Crystallogr. 44 (2011) 1272-1276.

[13] Sun, H. Pai, T. Nakamura, Y.-J. Shan, Y. Inaguma, M. Itoh, Ferroelectrics. 200 (1997) 93-107.

[14] S.K. Barik, R.N.P. Choudhary, P.K. Mahapatra, Appl. Phys. A. 88 (2007) 217-222.

[15] Y. Inaguma, J.-H. Sohn, I.-S. Kim, M. Itoh, T. Nakamura, J Phys Soc Jpn. 61 (1992) 3831-3832.

[16] A. Glazer, Acta Crystallogr B. 28 (1972) 3384-3392.

[17] A. Glazer, Acta Crystallographica Section A. 31 (1975) 756-762.

[18] J.J. Bian, K. Yan, J Electrocera. 21 (2007) 132-136.

[19] J.J. Bian, G.X. Song, K. Yan, Ceram. Int. 34 (2008) 893-896.

[20] Z. Fang, B. Tang, Y. Li, F. Si, S. Zhang, J Electron Mater. 44 (2015) 4236-4242.

[21] K. Hyun Yoon, E. Soo Kim, J.-S. Jeon, J Eur Ceram Soc. 23 (2003) 2391-2396.

[22] Z. Liang, L.L. Yuan, J.J. Bian, J Alloys Compd. 509 (2011) 1893-1896.

[23] J. Li, Y. Han, T. Qiu, C. Jin, Mater Res Bull. 47 (2012) 2375-2379.

[24] D. Zhou, C.A. Randall, H. Wang, L.-X. Pang, X. Yao, J Am Ceram Soc. 93 (2010) 1096-1100.

[25] Z.Q. Zheng, X.P. Zhou, J Am Ceram Soc. 96 (2013) 3504-3510.

[26] F. Guillemot, M.C. Porté, C. Labrugère, C. Baquey, J Colloid Interf Sci. 255 (2002) 75-78.

Fig. 1. Powder XRD patterns of $Na_{1/2}Sm_{1/2}TiO_3$ + *x* mol Cr_2O_3 ceramics (*x*=0~1.5%) sintered at 1450°C for 2 h in air

Fig. 2. Experimental (blue cross) and calculated (black line) X-ray powder diffraction profiles for $Na_{1/2}Sm_{1/2}TiO_3$ + *x* mol Cr_2O_3 ceramics sintered at 1450 °C for 2 h with (a) *x* =0 and (b) *x* =1%. The short vertical lines below the patterns mark the positions of Bragg reflections. The bottom continuous line is the difference between the observed and the calculated intensity

Fig. 3. Schematic representation of (a) $Na_{0.5}Sm_{0.5}TiO_3$ with perovskite structure and (b) the c-axis was chosen as the long axis

Fig. 4. SEM photographs of $Na_{0.5}Sm_{0.5}TiO_3$ + *x* mol Cr_2O_3 ceramics sintered at 1450 °C for 2 h with (a) *x*= 0 to (g) *x* = 1.5%.

Fig. 5. (a) Relative density, (b) Temperature coefficient of resonant frequency versus B-site bond valence (V_B), (c) dielectric constant and (d) Quality factor of $Na_{0.5}Sm_{0.5}TiO_3$ + *x* mol Cr_2O_3 ceramics (*x*=0 to 1.5%) sintered at 1450°C for 2 h.

Fig. 6. (a) The experimental XPS spectrum of Ti 2p for pure $Na_{0.5}Sm_{0.5}TiO_3$ and $Na_{1/2}Sm_{1/2}TiO_3$ + *x* mol Cr_2O_3 ceramics, and (b) the experimental and deconvoluted Ti 2p XPS spectrum for pure $Na_{0.5}Sm_{0.5}TiO_3$ ceramics sintered at 1450°C for 2 h.

Table 1. Refined crystal parameters and R values versus composition in $Na_{0.5}Sm_{0.5}TiO_3$ + *x* mol Cr_2O_3 ceramics (*x*=0 to 1.5%) sintered at 1450 °C for 2 h

Table 2. the representative chemical compositions of $Na_{0.5}Sm_{0.5}TiO_3$ + *x* mol Cr_2O_3 ceramic powder (*x*=0, 0.75% and 1.5%) sintered at 1450 °C for 2 h

Table 3. Theoretical density, relative density and polarizabilities of $Na_{0.5}Sm_{0.5}TiO_3$ + *x* mol Cr_2O_3 ceramics (*x*=0 to 1.5%) sintered at 1450 °C for 2 h

Table 4. B-site bond valence (V_B) and τ_f of $Na_{0.5}Sm_{0.5}TiO_3$ + *x* mol Cr_2O_3 ceramics (*x*=0 to 1.5%) sintered at 1450 °C for 2 h

Table 1. Refined crystal parameters and R values versus composition in $Na_{0.5}Sm_{0.5}TiO_3$ + *x* mol Cr_2O_3 ceramics (*x*=0 to 1.5%) sintered at 1450 °C for 2 h

x (mol)	0	0.25%	0.5%	0.75%	1%	1.25%	1.5%
a(Å)	3.82965	3.83039	3.8324	3.83166	3.83266	3.83269	3.83314
b(Å)	3.82398	3.82646	3.83076	3.83023	3.83315	3.8341	3.83447
c(Å)	3.83624	3.83681	3.8404	3.84073	3.84152	3.84231	3.84404
V (Å^3)	56.1798	56.2355	56.3868	56.4012	56.43639	56.4746	56.4867
Rw(%)	3.514467	3.810748	4.222899	4.5298953	4.7298953	4.9298953	5.7236986
Rwnb(%)	4.131237	4.5633874	4.603896	4.6214356	4.6414237	4.7214356	4.508272
Rb(%)	3.268523	3.2614727	3.281266	3.272021	3.472921	3.652372	3.7915907
Rexp(%)	3.101423	4.340112	4.309136	4.310237	4. 415289	4.618237	4.488856

Table 2. the representative chemical compositions of $Na_{0.5}Sm_{0.5}TiO_3$ + *x* mol Cr_2O_3 ceramic powder (*x*=0, 0.75% and 1.5%) sintered at 1450 °C for 2 h

Component	Sm_2O_3 (wt%)	TiO_2 (wt%)	Na_2O (wt%)	Cr_2O_3 (wt%)
0	44.697	43.96	9.929	0
0.75%	45.19	44.24	9.445	0.5857
1.5%	44.89	43.87	9.387	1.6586

Table 3. Theoretical density, relative density and polarizabilities of $Na_{0.5}Sm_{0.5}TiO_3$ + *x* mol Cr_2O_3 ceramics (*x*=0 to 1.5%) sintered at 1450 °C for 2 h

x (mol)	Theoretical density (g/cm^{-3})	Relative density (%)	V_m(Å^3)	Z	ε_γ	α/V_m
0.00	5.419	95.203	56.1798	1	99.6	0.23163
0.25%	5.396	95.803	56.2355	1	101.5	0.23181
0.5%	5.391	96.532	56.3868	1	100.7	0.23175
0.75%	5.377	96.652	56.4012	1	99.3	0.23166
1%	5.376	97.311	56.4364	1	95.95	0.23142
1.25%	5.373	95.566	56.4746	1	94.73	0.23132
1.5%	5.369	94.694	56.4867	1	93.66	0.23124

Table 4. B-site bond valence (V_B) and τ_f of $Na_{0.5}Sm_{0.5}TiO_3$ + *x* mol Cr_2O_3 ceramics (*x*=0 to 1.5%) sintered at 1450 °C for 2 h

x (mol)	$R_{Ti,Cr-O}$	$d_{Ti,Cr-O}$	b'	$V_{Ti,Cr-O}$	τ_f(ppm/°C)
0.00	1.815	1.914976	0.37	4.57933	199.3
0.25%	1.8236	1.915609	0.37	4.67851	187.2
0.5%	1.8321	1.917325	0.37	4.76584	184.6
0.75%	1.8407	1.917489	0.37	4.87523	175.1
1%	1.8492	1.917887	0.37	4.98396	171.2
1.25%	1.8578	1.91832	0.37	5.09465	165.4
1.5%	1.8664	1.918457	0.37	5.21196	160.8

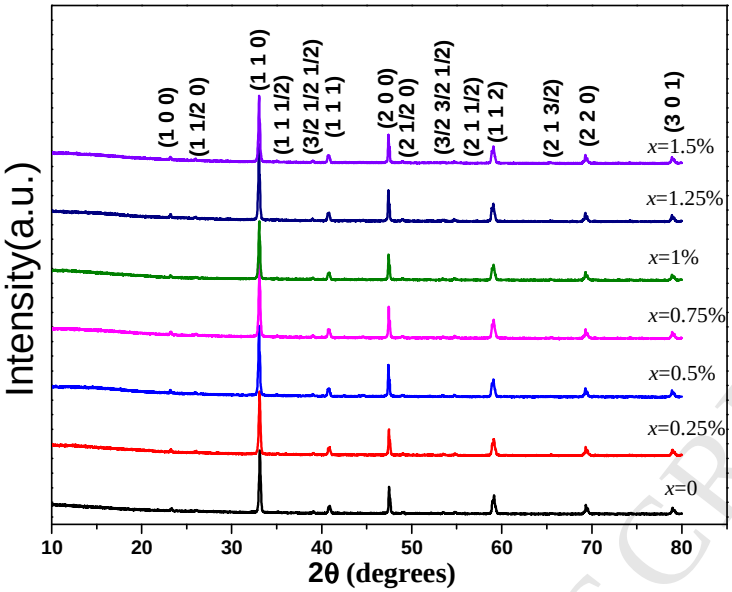

Fig. 1. Powder XRD patterns of $Na_{1/2}Sm_{1/2}TiO_3$ + *x* mol Cr_2O_3 ceramics (*x*=0 to 1.5%) sintered at 1450^{o}C for 2 h in air

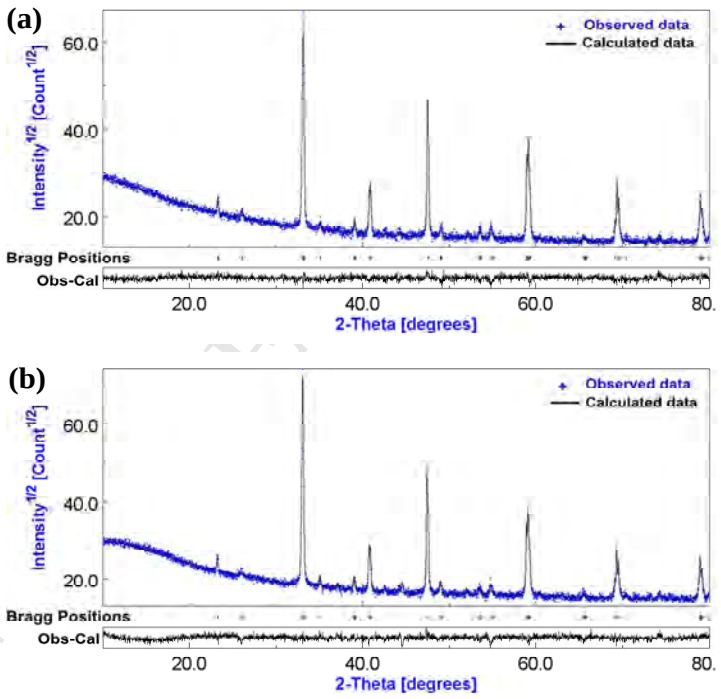

Fig. 2. Experimental (blue cross) and calculated (black line) X-ray powder diffraction profiles for $Na_{1/2}Sm_{1/2}TiO_3$ + *x* mol Cr_2O_3 ceramics sintered at 1450 ^{o}C for 2 h with (a) *x* =0 and (b) *x* =1%. The short vertical lines below the patterns mark the positions of Bragg reflections. The bottom continuous line is the difference between the observed and the calculated intensity

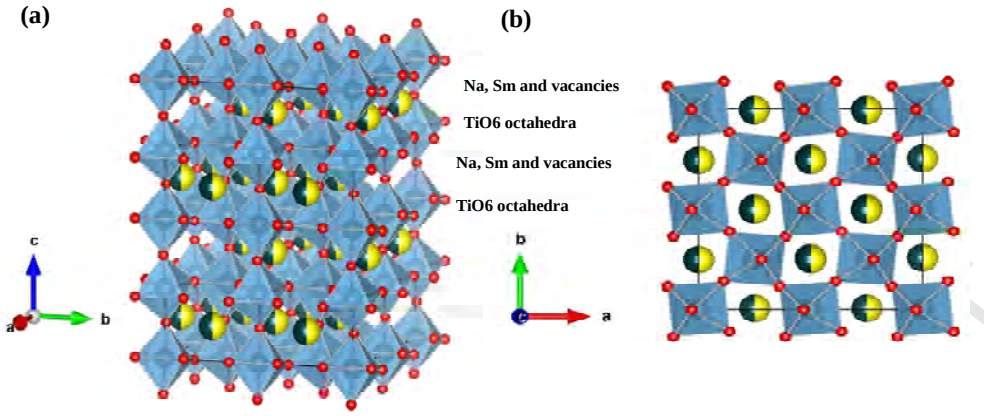

Fig. 3. Schematic representation of (a) $Na_{0.5}Sm_{0.5}TiO_3$ with perovskite structure and (b) the c-axis was chosen as the long axis

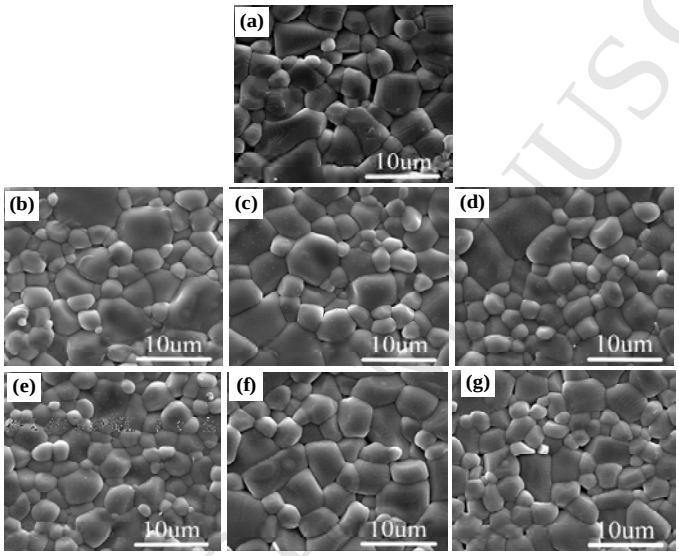

Fig. 4. SEM photographs of $Na_{0.5}Sm_{0.5}TiO_3$ + *x* mol Cr_2O_3 ceramics sintered at 1450 °C for 2 h with (a) *x*= 0 to (g) *x* = 1.5%.

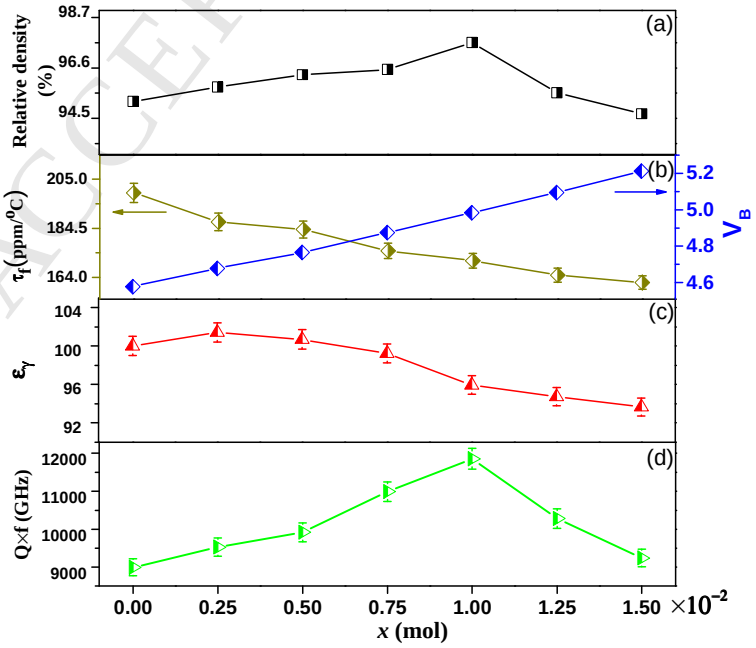

Fig. 5. (a) Relative density, (b) Temperature coefficient of resonant frequency versus B-site bond valence (V_B), (c) dielectric constant and (d) Quality factor of $Na_{0.5}Sm_{0.5}TiO_3$ + *x* mol Cr_2O_3 ceramics (*x*=0 to 1.5%) sintered at 1450°C for 2 h.

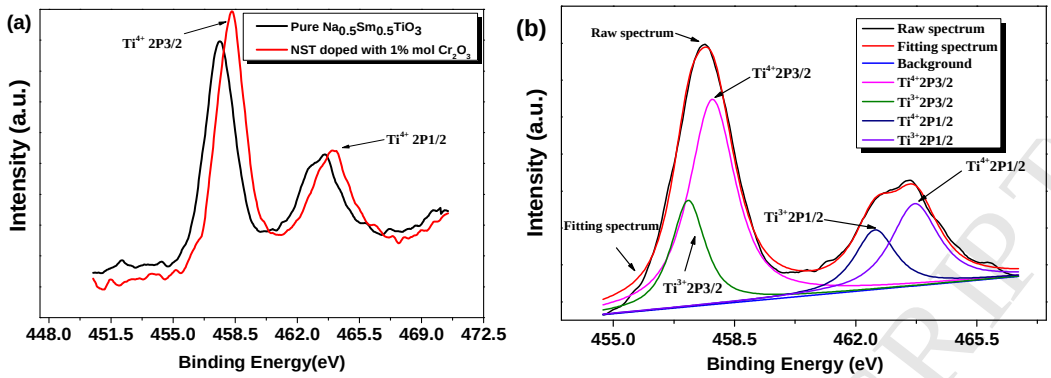

Fig. 6. (a) The experimental XPS spectrum of Ti 2p for pure $Na_{0.5}Sm_{0.5}TiO_3$ and $Na_{1/2}Sm_{1/2}TiO_3$ + *x* mol Cr_2O_3 ceramics, and (b) the experimental and deconvoluted Ti 2p XPS spectrum for pure $Na_{0.5}Sm_{0.5}TiO_3$ ceramics sintered at 1450°C for 2 h.

1. $Na_{0.5}Sm_{0.5}TiO_3$ + Cr_2O_3 ceramics were prepared by one process using the solid state method
2. The XPS results showed that Cr^{3+} substitution restrained the formation of Ti^{3+} ions.
3. The substitution of Cr^{3+} for Ti^{4+} would effectively lower the τ_f.
4. The substitution of Cr^{3+} for Ti^{4+} significantly improved the quality and maintained a high permittivity (ε_r=96, $Q\times f$=11854 GHz).